Nonlinear-process-induced period doubling of a picosecond transient grating in CdS

Hiroshi Saito and Akira Watanabe
Department of Applied Physics, Okayama University of Science, Ridai-cho 1-1, Okayama 700, Japan
(Received 7 October 1987)

The occurrence of higher-order Fourier components in an originally sinusoidal free-carrier index grating produced in CdS by the interference of two picosecond light pulses is demonstrated by monitoring simultaneously the temporal behavior of the first- and second-order diffraction intensities of transparent probe pulses for the temperature range 10–140 K. Nonlinear processes which take part in the decay of photoexcited carriers result in a deformation of the shape of the grating, which leads to the occurrence of higher-order Fourier components in the diffraction grating. Theoretical analysis of the experimental results yields the following distinct processes: bimolecular recombination of electrons and holes for the degenerate plasma, free-carrier–to–exciton Mott transition for the nondegenerate plasma at low carrier temperatures, and a nonlinear relation between exciton density and free-carrier density at high temperatures.

I. INTRODUCTION

Transient-induced grating experiments have been widely used to study the dynamics of diffusion, relaxation, and recombination of photoexcited carriers in solids.[1–4] In these experiments the interference of two coherent light pulses produces an intensity (absorption) or phase (index) grating inside a crystal which periodically modulates the optical properties of the material. The decay of this grating monitored by the diffraction of a third light pulse illustrates some of the intricacies of carrier dynamics. Information on phase-relaxation processes of photoexcited carriers can also be studied if the two interfering excitation pulses are delayed with respect to each other (four-wave mixing).[4,5]

The initially photoexcited sinusoidal grating remains sinusoidal at any time until it completely decays, if the dynamics of the photoexcited species responsible for the occurrence of a grating is described by linear processes only. The intensity of the diffracted beam in the first order provides full information on the decay of the grating for the purely sinusoidal intensity or phase grating. Nonlinear processes, on the contrary, result in a deformation of the shape of the grating, which leads to the occurrence of higher-order Fourier components in the diffraction grating and a modification of the diffraction pattern. Simultaneous observation of the decay of different diffraction orders is required to provide a more detailed insight into the dynamics of the photoexcited carrier system. To realize this concept we have performed picosecond transient-grating experiments in CdS.[6] The temporal behavior of a second-order Fourier component is revealed by simultaneous measurement of the decay of the first- and second-order diffraction intensities. This second-order grating is produced by nonlinear processes such as the bimolecular recombination of electrons and holes in the degnerate plasma and/or the formation of excitons in the nondegenerate first-order free-carrier grating (Mott transition). At elevated temperatures ($T > 60$ K) the exciton and the free carrier are in thermal equilibrium because of the thermal dissociation of exciton molecules. The nonlinear relation between the exciton density and the free-carrier density also brings about second-order Fourier components. Further increase in temperature ($T > 140$ K) makes the exciton contribution negligible, and in fact no higher-order components are observed.

In this paper, the theory as well as the experimental results are discussed. Section II describes the theoretical background for calculation of the diffraction intensity of different orders in the Raman-Nath regime. In Sec. III are shown the experimental procedures for transient-grating measurements. Section IV deals with the discussion of the experimental results. The decay mechanisms of the photoexcited carriers can be determined by comparing the experimental data with the theoretical calculations.[7]

II. THEORETICAL BACKGROUND

A. Diffraction in the Raman-Nath regime

The diffraction of the probe beam is due to the spatially periodic change of the refractive index of the sample induced by free carriers or excitons. The index change due to the photoexcited free carriers can be estimated within the limits of the Drude model. The exciton contribution is calculated by using a simple-harmonic-oscillator (Lorentz) model.[8] In both cases the index change is proportional to the carrier or the exciton density. Nonlinear processes which take part in the decay of the grating will result in the deformation of the free-carrier distribution from the initially created sinusoidal shape. Let $\Delta N_j(\Lambda_j)$ be the difference of the free-carrier density at the peak of the grating and its minimum for the jth Fourier component of the carrier distribution with the grating spacing of Λ_j. The amplitude of the jth Fourier component of the index change, Δn_j, owing to $\Delta N_j(\Lambda_j)$ is then given by

$$\Delta n_j = -\frac{e^2}{2m^*\omega_s^2\epsilon_0 n_0}\Delta N_j(\Lambda_j) , \tag{1}$$

where ω_s is the angular frequency of the probe pulse, n_0 is the background refractive index at ω_s, e is the electron charge, ϵ_0 is the permittivity in vacuum and m^* is the reduced mass of the electron (effective mass of m_e) and the hole effective mass of m_h). For m_h we use the density-of-states mass of $m_{h\parallel}$ and $m_{h\perp}$, where $m_{h\parallel}$ and $m_{h\perp}$ are the effective hole masses parallel and perpendicular to the c axis of CdS, respectively.[9] As will be consequently shown, Λ_j is given by $\Lambda_j=\Lambda/j$, where Λ represents the spacing of the initially created grating and corresponds to the $j=1$ Fourier component. The exciton contribution to Δn_j is given by a relation similar to Eq. (1) in which ω_s^2 in the denominator is replaced by $\omega_{ex}^2-\omega_s^2$, where ω_{ex} is the angular frequency of the free exciton. Hence, Δn_j becomes larger than the free-carrier contribution for equal density.

For incident probe beam normal to the grating in the Raman-Nath regime ($\phi_n \ll 1$), the amplitude of the nth order diffraction light, ϕ_n, due to Δn_j is given by the solution of the difference-differential equation,[10]

$$\frac{d\phi_n}{dz}+\frac{\Phi_j}{2L}(\phi_{n-j}-\phi_{n+j})=0 , \tag{2}$$

where z is the direction normal to the grating and Φ_j is the phase modulation of the probe pulse at wavelength λ_s due to Δn_j, and is defined for the grating with thickness L by

$$\Phi_j=\frac{2\pi L}{\lambda_s}\Delta n_j . \tag{3}$$

The solution of Eq. (2) is given by the Bessel function of the nth order, i.e., $\phi_n=J_n(\Phi_j)$. The phase modulation Φ_j, which takes the maximum value for $j=1$, is at most $\sim 3.6\times 10^{-2}$, calculated using Eqs. (1) and (3) for $\lambda_s=532$ nm, $L=1$ μm, and $\Delta N_1(\Lambda)=10^{25}$ m^{-3} ($=10^{19}$ cm^{-3}). The relation $\Phi \ll 1$ thus holds, resulting in $\phi \ll 1$; i.e., the grating is surely in the Raman-Nath regime. The nth order Bessel function can then be approximated by $(\Phi_j/2)^n/n!$. The intensity of the nth diffraction order due to the jth Fourier component of the refractive index change, $I_{dif}^{(n)}(\Lambda_j)$, is given by

$$I_{dif}^{(n)}(\Lambda_j)=\left[\left[\frac{\Phi_j}{2}\right]^n\frac{1}{n!}\right]^2=\left[\frac{C^n}{n!}\right]^2[\Delta N_j(\Lambda_j)]^{2n} , \tag{4}$$

where

$$C=\frac{\pi L e^2}{2m^*\lambda_s\omega_s^2\epsilon_0 n_0}$$

from Eqs. (1) and (3).

The temporal behavior of $I_{dif}^{(n)}(\Lambda_j)$ can be calculated directly from the time dependence of $\Delta N_j(\Lambda_j)$. For a purely sinusoidal grating ($j=1$ only), Eq. (4) leads to the fact that the decay time of the second-order diffraction intensity, $I_{dif}^{(2)}(\Lambda)$, is just half of the decay time of the first-order intensity, $I_{dif}^{(1)}(\Lambda)$. In other words, the time dependence of the ratio of $I_{dif}^{(2)}(\Lambda)$ to $I_{dif}^{(1)}(\Lambda)$, i.e., $I_{dif}^{(2)}(\Lambda)/I_{dif}^{(1)}(\Lambda)$, becomes just the same as that of $I_{dif}^{(1)}(\Lambda)$. It is also noted that the value of this ratio is at most of the order of 10^{-5} for $\Delta N_1(\Lambda)=10^{19}$ cm^{-3}.

The carrier density and, therefore, the index change have a steep gradient inside the sample because of large absorption coefficient of the order of 10^5 cm^{-1}. Strictly speaking the phase modulation Φ_j can not be simply given by the product of L and Δn_j [Eq. (3)], but instead is proportional to the integration of Δn_j from the front to the rear surface of the sample. It should be noted, however, that the diffraction of the probe beam is dominated by the carrier distribution close to the surface where the density is highest.[11] For this reason as well as for facility of the following calculation, we neglect the concentration gradient inside the crystal, and assume instead an averaged distribution within the depth corresponding to the inverse of the absorption coefficient.

B. Calculation of $\Delta N_j(\Lambda_j)$

1. At low temperatures

In the case of nonuniform excitation, excitons, exciton molecules, and free carriers coexist. At high excitation intensities the exciton binding is screened at the maxima of the grating where the free-carrier density is highest. Excitons and exciton molecules are preferably formed at the minima of the grating where the free-carrier density is lowest. At carrier temperatures approximately below 60 K for CdS, exciton molecules are thermally stable. Very fast recombination of exciton molecules results in the fact that the exciton density becomes negligibly small even at the minima of the grating. Thus we consider the temporal and spatial change of the free carrier density only, neglecting the excitonic contribution.

Free carrier plasma grating decays due to either bimolecular recombination and diffusion or free-carrier–to–exciton Mott transition and diffusion depending on the plasma being in the degenerate or nondegenerate state, respectively. Note that the Mott transition is also a bimolecular process. The density of electron-hole pairs at the position x along the sample surface and at time t, $N_{e\text{-}h}(x,t)$, is then given by the solution of the continuity equation,

$$\frac{\partial N_{e\text{-}h}(x,t)}{\partial t}=-\beta N^2(x,t)+D\frac{\partial^2 N_{e\text{-}h}(x,t)}{\partial x^2} , \tag{5}$$

where D is the ambipolar diffusion coefficient and is assumed to be density (and therefore position) independent, and β is the rate of the bimolecular process. In solving Eq. (5), we assume that the excitation of the grating is given by the delta function at $t=0$, i.e., $N_{e\text{-}h}(x,0)=N_0[1+\cos(2\pi x/\Lambda)]/2$, where N_0 is the pair density at $x=0$ (peak of the grating) and $t=0$. Equation (5) can be solved analytically only when $D=0$, giving rise to

$$N_{e\text{-}h}(x,t)=N_0\frac{1+\cos(2\pi x/\Lambda)}{2+\tilde{\beta}t[1+\cos(2\pi x/\Lambda)]} , \tag{6}$$

where $\tilde{\beta}=\beta N_0$. In the case of $D\neq 0$, we assume that the carrier diffusion affects only the modulation of the carrier distribution which is represented by the cosine terms in Eq. (6) to decay exponentially, i.e., $\exp(-\gamma t)$, where γ is

the decay rate of the grating due to carrier diffusion and is assumed to be $\gamma = D(2\pi/\Lambda)^2$. As will be subsequently shown this γ value is obtained in the case that the carriers recombine by linear process. An approximate solution for Eq. (5) is

$$N_{e\text{-}h}(x,t) = N_0 \frac{1+\exp(-\gamma t)\cos(2\pi x/\Lambda)}{2+\tilde{\beta} t[1+\exp(-\gamma t)\cos(2\pi x/\Lambda)]} . \quad (7)$$

This approximation is applicale only when the diffusion effect is less efficient than the bimolecular process. Expansion in a Fourier series is performed only for the denominator of Eq. (7), owing to the fact that analytical expansion of Eq. (7) as a whole is not possible and also that the deformation from the sinusoidal shape is brought about by the denominator. $N_{e\text{-}h}(x,t)$ can be expressed as

$$N_{e\text{-}h}(x,t) = N_0(\{1 - B\exp(-\gamma t)\} + \{[1 - 2B\exp(\gamma t) + B^2]\exp(-\gamma t)\cos(2\pi x/\Lambda)\} - \{B[1 - 2B\exp(\gamma t) + B^2]\exp(-\gamma t)\cos(4\pi x/\Lambda)\} + \cdots)/A , \quad (8)$$

where

$$A = [(2+\tilde{\beta} t)^2 - (\tilde{\beta} t)^2\exp(-2\gamma t)]^{1/2} ,$$

and

$$B = \frac{2+\tilde{\beta} t - A}{\tilde{\beta} t \exp(-\gamma t)} .$$

The quantity in the first set of curly brackets in Eq. (8) represents the term with constant carrier density. The first-Fourier component [$j=1$; the second set of curly brackets in Eq. (8)] yields $\Delta N_1(\Lambda)$, the difference of the carrier density at the peak ($x=0$) and its minimum ($x=\Lambda/2$). Using Eq. (4) the first-order diffraction intensity due to the Λ grating, $I^{(1)}_{\text{dif}}(\Lambda)$, is given by

$$I^{(1)}_{\text{dif}}(\Lambda) = [C\Delta N_1(\Lambda)]^2 = [CN_0(1 - 2B\exp(\gamma t) + B^2)\exp(-\gamma t)/A]^2 . \quad (9)$$

For the $j=2$ term [the third set of curly brackets in Eq. (8); $\Lambda/2$ grating], the carrier occupies the peak density at $x=\Lambda/4$ and the minimum density at $x=0$. [Note the negative sign for the $j=2$ term in Eq. (8).] Therefore, the first-order diffraction intensity due to the $\Lambda/2$ grating, $I^{(1)}_{\text{dif}}(\Lambda/2)$, becomes

$$I^{(1)}_{\text{dif}}(\Lambda/2) = [C\,\Delta N_2(\Lambda/2)]^2 = [CN_0(1 - 2B\exp(\gamma t) + B^2)\exp(-\gamma t)B/A]^2 . \quad (10)$$

The ratio of $I^{(1)}_{\text{dif}}(\Lambda/2)$ to $I^{(1)}_{\text{dif}}(\Lambda)$ becomes

$$\frac{I^{(1)}_{\text{dif}}(\Lambda/2)}{I^{(1)}_{\text{dif}}(\Lambda)} = B^2 = \left[\frac{2+\tilde{\beta} t - [(2+\tilde{\beta} t)^2 - (\tilde{\beta} t)^2\exp(-2\gamma t)]^{1/2}}{\tilde{\beta} t \exp(-\gamma t)}\right]^2 . \quad (11)$$

It is to be noted that the ratio [Eq. (11)] is determined only by the $\tilde{\beta}$ and γ values, and does not include the initial carrier density N_0 nor any other material parameters shown in Eq. (1).

Figure 1 depicts the time dependence of the calculated ratio, $I^{(1)}_{\text{dif}}(\Lambda/2)/I^{(1)}_{\text{dif}}(\Lambda)$, for three Λ values; $\Lambda = 7.9$ μm by solid curves, $\Lambda = 4.0$ μm by dotted curves and $\Lambda = 2.9$ μm by dash-dotted curves, each for $\tilde{\beta} = 2\times10^9$ s^{-1} and $D = 3$ cm^2/s, $\tilde{\beta} = 1\times10^{10}$ s^{-1} and $D = 3$ cm^2/s, and $\tilde{\beta} = 1\times10^{10}$ s^{-1} and $D = 7$ cm^2/s. Equation (11) indicates that for $D = 0$ (or $\Lambda = \infty$) the decay of $I^{(1)}_{\text{dif}}(\Lambda/2)$ is always slower than the decay of $I^{(1)}_{\text{dif}}(\Lambda)$, i.e., the ratio increases monotonously with time delay as shown by the dashed curve for the respective $\tilde{\beta}$ values. Owing to the fact that the period doubling of the grating is brought about by a nonlinear process, the value of the ratio decreases if the contribution of the nonlinear process becomes small compared with the effect of the carrier diffusion as in the following cases: (1) the case of smaller $\tilde{\beta}$ values for the given D and Λ values (cf. the case of $\tilde{\beta} = 1\times10^{10}$ s^{-1} and $\tilde{\beta} = 2\times10^9$ s^{-1} for $D = 3$ cm^2/s), (2) the case of larger D values for the given $\tilde{\beta}$ and Λ values (cf. the case of $D = 7$ cm^2/s and $D = 3$ cm^2/s for $\tilde{\beta} = 1\times10^{10}$ s^{-1}), and (3) the case of smaller Λ values for the given $\tilde{\beta}$ and D values. Moreover, the ratio has somewhat similar temporal behavior among the different Λ values in case of smaller D value because of insufficient diffusion effect (cf. the case of $D = 7$ cm^2/s and $D = 3$ cm^2/s).

2. *At high temperatures*

At temperatures above about 60 K in CdS, where the exciton molecule is thermally dissociated, the main channel which diminishes the exciton density disappears.[12] This results in the occurrence of thermal equilibrium between the exciton and the free carrier. Under this condition, the exciton density, N_{ex}, is proportional to the square of the free carrier density, $N_{e\text{-}h}$, i.e.,

$$N_{\text{ex}} = \eta N^2_{e\text{-}h} , \quad (12)$$

where η is a function of temperature and the exciton

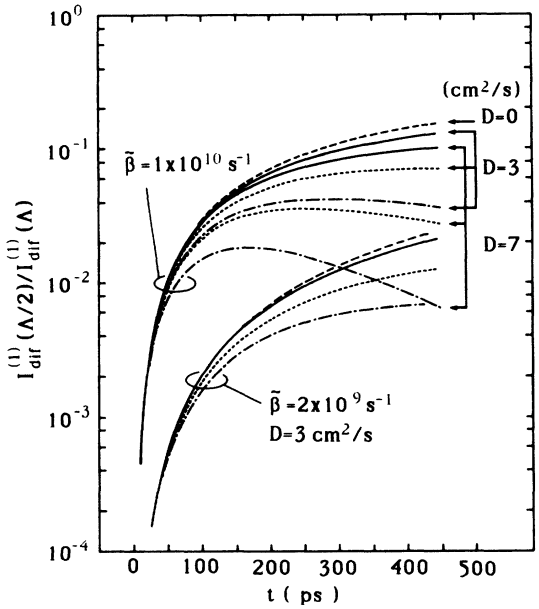

FIG. 1. Time dependence of calculated ratio of the first-order diffraction intensity due to the grating with $\Lambda/2$ spacing, $I^{(1)}_{dif}(\Lambda/2)$, to that due to the grating with Λ spacing, $I^{(1)}_{dif}(\Lambda)$, $I^{(1)}_{dif}(\Lambda/2)/I^{(1)}_{dif}(\Lambda)$, for three grating spacings; $\Lambda=7.9$ μm (solid curves), $\Lambda=4.0$ μm (dotted curves), $\Lambda=2.9$ μm (dash-dotted curves). Dashed curves indicate the case of no diffusion ($D=0$).

binding energy, and decreases with increasing temperature.[13] It should be noted that this nonlinear relation between N_{ex} and $N_{e\text{-}h}$ also brings about the exciton grating with $\Lambda/2$ spacing.

In the following calculation, we again assume that the exciton density is much less than the free carrier density, and that the latter decays by linear process with the rate of Γ. The temporal and spatial change of the free carrier density, $N_{e\text{-}h}(x,t)$, is then given by

$$N_{e\text{-}h}(x,t)=N_0[1+\cos(2\pi x/\Lambda)\exp(-\gamma t)] \times\exp(-\Gamma t)/2 , \quad (13)$$

where the same initial condition as that in solving Eq. (5) is used. The first-order diffraction intensity due to the free carrier grating with spacing Λ is

$$I^{(1)}_{dif}(\Lambda)=(CN_0)^2\exp(-2\Gamma^* t) , \quad (14)$$

where $\Gamma^*=\gamma+\Gamma=D(2\pi/\Lambda)^2+\Gamma$.

As will be discussed in Sec. IV C, exciton diffusion can be neglected, i.e., the exciton grating decays only due to recombination, while the free carrier grating decays due to both recombination and diffusion. This fact suggests that any alteration to the free-carrier distribution in Eq. (13) is not necessary even if we take the exciton contribution into consideration. The exciton density is then given by the square of the free-carrier density, but should decay in the same manner as that of $N_{e\text{-}h}$ [Eq. (13)] because of the thermal equilibrium existing between them. The first-order diffraction intensity due to the exciton grating can be expressed as

$$I^{(1)}_{dif}(\Lambda/2)=C^2\eta^2N_0^4\exp(2\Gamma^* t) . \quad (15)$$

The ratio of $I^{(1)}_{dif}(\Lambda/2)$ to $I^{(1)}_{dif}(\Lambda)$ becomes

$$I^{(1)}_{dif}(\Lambda/2)/I^{(1)}_{dif}(\Lambda)=(\eta N_0)^2 . \quad (16)$$

In the present approximation the value of the ratio becomes independent of Λ. Because η should increase with decreasing temperature, the ratio increases for lower carrier temperature and higher I_{exc}, in spite of the fact that the absolute value can not be determined.

With further increase of the temperature, the exciton density becomes negligibly small because of thermal dissociation. The deformation from the sinusoidal grating can then be neglected, i.e., no higher-order Fourier components result. The observed second-order diffraction intensity should certainly correspond to the second-order diffraction due to the Λ grating.

III. EXPERIMENTAL PROCEDURES

The experimental configuration used is as follows: Two excitation pulses with a wavelength of 355 nm, the third-harmonic pulses of an active-passive mode-locked Nd:YAG laser (pulse width 25 ps), separated by an angle of 2θ, are focused on the sample to coincide both spatially and temporally (Fig. 2). The interference between the two pump pulses produces a modulation of the optically excited free-carrier density at the sample surface, which is proportional to $1+\cos(2\pi x/\Lambda)$, where the x direction is taken along the sample surface, and Λ is the grating spacing given by $\Lambda=\lambda_p/(2\sin\theta)$ (λ_p is the pump-pulse wavelength). This grating decays in time due to recombination, transformation into excitons, and diffusion of the carriers. The grating decay is monitored by measuring the first-order, $I^{(1)}_{dif}$, and the second-order diffracted light, $I^{(2)}_{dif}$, of the second-harmonic pulses ($\lambda_s=532$ nm) of the Nd:YAG laser as a function of time delay between the excitation pulses and the probe pulses. The probe pulses at $\lambda_s=532$ nm is transparent for CdS. The angle of the jth order diffracted beam due to the grating with the spacing Λ, $\varphi^{(j)}$, is given by $\sin\varphi^{(j)}=j\lambda_s/\Lambda$. It is noted, therefore, that the second-order diffracted beam due

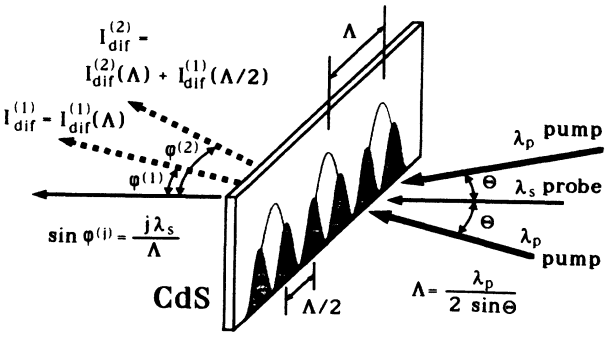

FIG. 2. Schematics of experimental technique for producing and measuring transient grating. $I^{(1)}_{dif}$ and $I^{(2)}_{dis}$ are the first- and second-order diffracted beams, respectively.

to the Λ grating just coincides with the first-order diffracted beam due to the $\Lambda/2$ grating (see Fig. 2).

A single pulse is switched from the train of the mode-locked pulses by means of an electrooptic shutter. Excitation pulses and probe pulses with almost constant amplitude are selected electronically and are used for averaging. The excitation energy, I_{exc}, of 1 μJ corresponds to a power density of about 10 MW/cm^2. Thin platelet crystals of 10–50 μm thickness are used. The temperature of the crystals mounted on a cold finger which is in contact with liquid He is controllable from 10 K up to about 200 K within an accuracy of ± 2 K during experiments.

IV. EXPERIMENTAL RESULTS AND DISCUSSION

A. Results at $T_{bath} \leq 40$ K

Experimental results for the diffraction intensity versus time delay measured at the bath temperature of $T_{bath} = 10$ K are summarized in Fig. 3 for three grating spacings. The filled and open circles correspond to the first-order [$I_{dif}^{(1)}$] and second-order [$I_{dif}^{(2)}$] diffracted beams, respectively. The intensity scale for $I_{dif}^{(2)}$ is shifted with respect to $I_{dif}^{(1)}$, so that the data for $I_{dif}^{(1)}$ and those for $I_{dif}^{(2)}$ nearly coincide in the later time regime for each Λ. The decay of $I_{dif}^{(1)}$ can be characterized by a fast initial and a slower component in the later time regime. The temporal position of the maximum of $I_{dif}^{(1)}$ remains nearly constant for different Λ. The decay of $I_{dif}^{(2)}$ is nearly exponential and the peak position shifts to longer delay times with increasing Λ. The decay times become faster with decreasing Λ as a result of the carrier diffusion. It is important to note that roughly the same decay time observed in the later time regime for $I_{dif}^{(1)}$ and $I_{dif}^{(2)}$ leads to the fact that the time dependence of $I_{dif}^{(2)}$ cannot be simply described by the second-order diffraction due to a sinusoidal grating with spacing Λ [cf. Eq. (4)].

Solid curves in Fig. 3 represent $I_{dif}^{(1)}(\Lambda)$ and $I_{dif}^{(1)}(\Lambda/2)$ calculated for $\tilde{\beta} = 1.2 \times 10^{10}$ s^{-1} and $D = 8$ cm^2/s using Eqs. 9 and 10, respectively.[14] The absolute values for both $I_{dif}^{(1)}(\Lambda)$ and $I_{dif}^{(1)}(\Lambda/2)$ are shifted so as to fit the experimental points. In any case, fairly good agreement both for the first- and second-order components is found in the time regime later than approximately 100 ps.

In order to discuss in detail the relation of diffraction intensities between the different diffraction orders and those between the different Λ values, it is rather convenient to plot the ratio of the diffraction intensity in the second order to that in the first order, $I_{dif}^{(2)}/I_{dif}^{(1)}$, instead of the diffraction intensity itself as in Fig. 3. Figure 4 depicts experimental data for the ratio $I_{dif}^{(2)}/I_{dif}^{(1)}$ versus time delay for the same data as shown in Fig. 3: $\Lambda = 7.9$ μm (open circles), $\Lambda = 4.0$ μm (solid circles) and $\Lambda = 2.9$ μm (squares). One can clearly recognize that the decay of $I_{dif}^{(2)}$ is slower than that of $I_{dif}^{(1)}$ for $\Lambda = 7.9$ μm, nearly equal for $\Lambda = 4.0$ μm and somewhat faster for $\Lambda = 2.9$ μm. The ra-

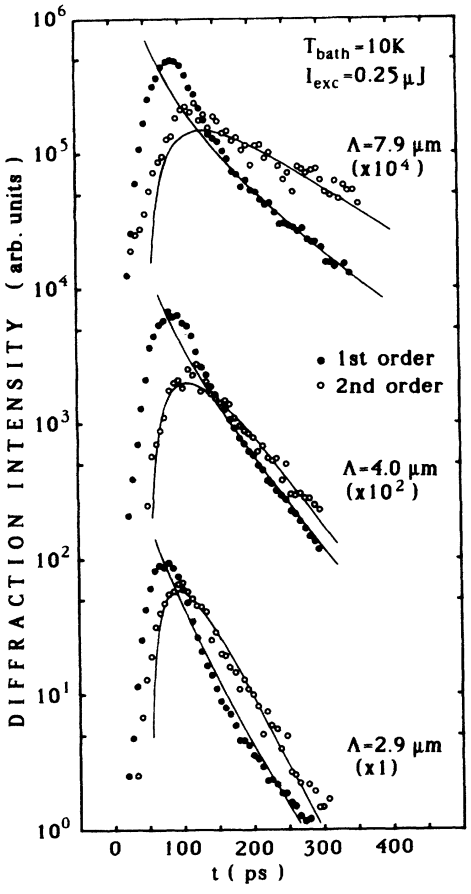

FIG. 3. Observed diffraction intensity in the first (solid circles) and second order (open circles) as a function of time delay for three grating spacings measured at $T_{bath} = 10$ K. Solid curves are the calculated diffraction intensities for $\tilde{\beta} = 1.2 \times 10^{10}$ s^{-1} and $D = 8$ cm^2/s as described in the text.

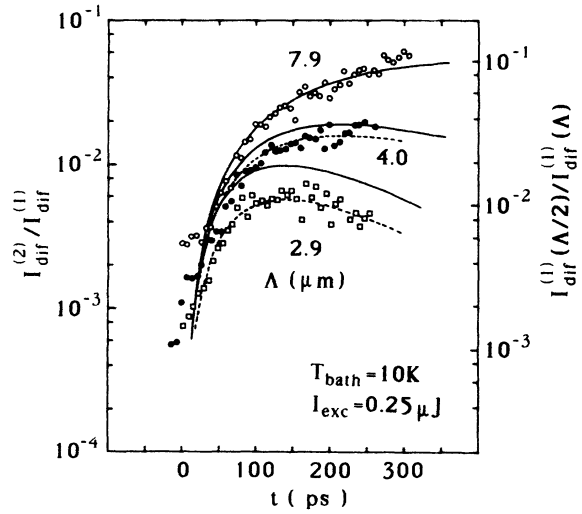

FIG. 4. Observed ratio, $I_{dif}^{(2)}/I_{dif}^{(1)}$, as a function of time delay measured at $T_{bath} = 10$ K for three grating spacings; $\Lambda = 7.9$ μm (open circles), $\Lambda = 4.0$ μm (solid circles) and $\Lambda = 2.9$ μm (squares). Solid and dashed curves indicate the calculated ratio, $I_{dif}^{(1)}(\Lambda/2)/I_{dif}^{(1)}(\Lambda)$, for $\tilde{\beta} = 1.2 \times 10^{10}$ s^{-1} and $D = 8$ cm^2/s as described in the text.

tio has a larger value for larger Λ value. The solid curves in Fig. 4 are the calculated results of the ratio, $I_{dif}^{(1)}(\Lambda/2)/I_{dif}^{(1)}(\Lambda)$, for the same $\tilde{\beta}$ and D values as in Fig. 3; $\tilde{\beta}=1.2\times10^{10}$ s^{-1} and $D=8$ cm^2/s. The ordinate scale for the calculated results, however, is shifted so that the calculated curve for $\Lambda=7.9$ μm coincides with the experimental points for $\Lambda=7.9$ μm. (The ordinate scale on the right-hand side is for the calculated ratio and that on the left-hand side for the observed ratio.) The calculated ratio is found to be about 2 times larger than the experimentally obtained ratio. This discrepancy increases with decreasing Λ. The dashed curves for $\Lambda=4.0$ and 2.9 μm are also the calculated results but are shifted so as to fit well to the respective data points. It is noted that agreement between the experimental and calculated results is good as far as the time-dependence of the ratio is concerned. Similar results are obtained for $I_{exc}=0.18$ and 0.5 μJ, and also for three I_{exc}'s measured at $T_{bath}=40$ K. The results of the theoretical analysis are summarized in Table I.

The discrepancy between the experimental and the calculated ratios in Fig. 4 is ascribed to the approximation presently used. The approximate solution for $N_{e\text{-}h}(x,t)$ in Eq. (7) gives rise to the carrier density at $x=\Lambda/4$, $N_{e\text{-}h}(\Lambda/4,t)=N_0/(2+\tilde{\beta}t)$, which is independent of the D value, i.e., the carrier density at $\Lambda/4$ decreases only by the bimolecular recombination or the transformation process, and is not affected by the carrier diffusion. This result, however, is not correct for the actual distribution of the carrier. Numerical solution of Eq. (5) shows that the carrier density at $x=\Lambda/4$ becomes smaller than that of the approximate value obtained from Eq. (7) irrespective of $\tilde{\beta}$ and D values for the entire time range measured here. This fact leads to the overestimation of the calculated $I_{dif}^{(1)}(\Lambda/2)$ value, resulting in the larger value for the ratio. This discrepancy becomes larger for smaller Λ value, where the diffusion effect is more efficient and therefore the approximation becomes worse.

In the present calculation of the diffraction intensities, we employed the initial condition that the excitation of the grating is given by the delta function at $t=0$. Inclusion of the correct pulse shape, however, enhances further the discrepancy between the experimental and calculated results in the earlier time regime (Fig. 3), indicating that the plasma grating in the earlier time regime decays with larger $\tilde{\beta}$ value than that obtained here. This fact is in accordance with our previous experiments where degenerate electron-hole plasma decays very fast by bimolecular recombination with the rate of $\beta=(5-7)\times10^{-9}$ cm^3/s corresponding to $\tilde{\beta}=(1-1.4)\times10^{11}$ s^{-1} for the initial plasma density of 2×10^{19} cm^{-3}, and changes into nondegenerate plasma at 100–150 ps after the excitation. Thereafter, optical gain as well as a luminescence line due to the recombination of exciton molecules are observed.[11] For nondegenerate plasma the recombination of free carriers is of minor importance, and the recombination of exciton molecules determines the decay of the free carrier and the exciton system.[15] Present $\tilde{\beta}$ values listed in Table 1 are about one-order of magnitude smaller than those for degenerate plasma and correspond to nondegenerate plasma. Taking these facts into consideration we can conclude that the $\tilde{\beta}$ values presently obtained are determined mainly by the free-carrier–exciton Mott transition.

TABLE I. Obtained $\tilde{\beta}$, Γ, and D values. Note that the data in the parentheses at $T_{bath}=60$ K are obtained for $I_{exc}=0.35$ μJ. $\tilde{\beta}$ and Γ are in units of 10^9 s^{-1}; D is in units of cm^2/s.

I_{exc} (μJ)		10 K	40 K		60 K
0.18	$\tilde{\beta}$	10–12	8–10	Γ	~0.8
	D	~7	5.5–6	D	~2
0.25	$\tilde{\beta}$	12–13	10–12	Γ	~1
	D	8–9	6.5–7	D	~4
0.5	$\tilde{\beta}$	~15	~12	Γ	(~1)
	D	~10	~8	D	(~5)

B. Results at $T_{bath}\geq 60$ K

Figure 5 shows experimental data for the ratio $I_{dif}^{(2)}/I_{dif}^{(1)}$, measured at $T_{bath}=60$ and 70 K for three excitation intensities and for three Λ values: 7.9, 4.0, and 2.9 μm. (The diffraction intensity for $I_{exc}=0.18$ μJ at $T_{bath}=75$ K is too weak to be measured.) The decay of $I_{dif}^{(1)}$ itself, although not shown, is characterized by a fast initial and a slower exponential component in the time regime later than 100 ps, whereas the decay of $I_{dif}^{(2)}$ is exponential in the entire time regime with nearly the same time constant as that for $I_{dif}^{(1)}$, giving rise to the results in the later time regime shown in Fig. 5. According to the theoretical prediction in Eq. (4), the time dependence of $I_{dif}^{(2)}$ again cannot be described by the second-order diffraction due to a sinusoidal grating. All of the observed ratios show almost no time dependence in the time regime later than about 100 ps. This fact is different from the observed data at lower temperatures (cf. Fig. 4). Note

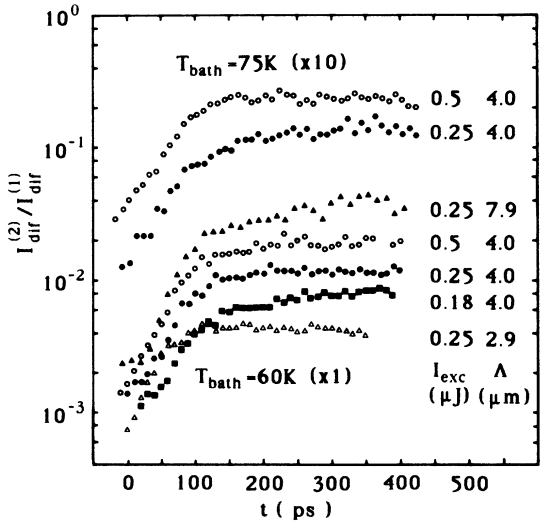

FIG. 5. Observed ratio $I_{dif}^{(2)}/I_{dif}^{(1)}$ as a function of time delay measured at $T_{bath}=60$ and 75 K for three excitation intensities and for three grating spacings.

that the value of the ratio increases with increasing I_{exc} and decreases with increasing temperature for the corresponding I_{exc}. These results are in accordance with the theory for higher temperatures [Eq. (16), Sec. II B 2]; the ratio has no time dependence but increases with increasing N_0 and η, corresponding to higher I_{exc} and lower temperature, respectively. The value of the ratio, however, increases with increasing Λ, which is in contradiction to the present theory in which the value of the ratio is independent of the Λ value.

For comparison we also performed the calculation of the ratio using Eq. (11). In the case of smaller D value the ratio shows somewhat similar temporal behavior among the different Λ values because of insufficient diffusion effect (cf. Fig. 1). This resembles the observed data in Fig. 5. For smaller $\tilde{\beta}$ value, however, the absolute value for the ratio decreases considerably, especially in the time regime earlier than about 150 ps. It is found that no calculations fit well to the experimental results. This fact provides further confirmation to the interpretation that the exciton molecule is already thermally dissociated, and the thermal equilibrium is established between the exciton and the nondegenerate free carrier at these temperatures.[12] By analyzing the exponential decay component of $I_{dif}^{(1)}$ observed in the later time regime for $T_{bath}=60$ K using Eq. (14), we obtained the D and Γ values as listed also in Table I.

Figure 6 depicts experimental results for $T_{bath}=140$ K. The solid and open circles correspond to the first- and second-order diffracted beams, respectively. Both signals decay exponentially, with decay constants of 540 and 270 ps for $I_{dif}^{(1)}$ and $I_{dif}^{(2)}$, respectively. In Fig. 6 the ratio of the second-order to the first-order diffraction intensity, $I_{dif}^{(2)}/I_{dif}^{(1)}$, is also plotted (see open squares). The solid line indicates the exponential decay with the same time constant for $I_{dif}^{(1)}$, i.e., 540 ps, and is found to fit well to the experimental points for the ratio. At this temperature the exciton density becomes negligibly small because of thermal dissociation. The deformation from the sinusoidal grating can then be neglected, i.e., no higher-order Fourier components result. Thus the observed results are in perfect agreement with the theoretical predictions for an ideal sinusoidal grating.

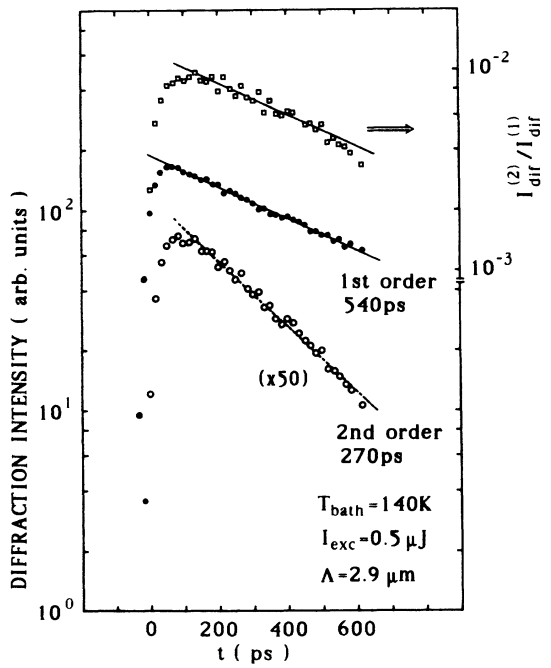

FIG. 6. Observed diffraction intensity in the first-order, $I_{dif}^{(1)}$ (solid circles) and the second-order, $I_{dif}^{(2)}$ (open circles), and the ratio $I_{dif}^{(2)}/I_{dif}^{(1)}$ (squares) as a function of time delay for $\Lambda=2.9$ μm measured at $T_{bath}=140$ K. Solid and dotted lines indicate the exponential decay with the time constant of 540 and 270 ps, respectively.

C. DISCUSSION ON D VALUES

Free carriers suffer several kinds of scatterings, e.g., polar-optical(LO)-phonon, acoustic-phonon, piezoelectric and impurity scatterings.[16] At the effective carrier temperature T_{eff}, below ~ 50 K, the piezoelectric and impurity scatterings dominate the processes which determine the mobility of free carriers in CdS. At $T_{eff}>70$ K, on the other hand, the carrier mobility is determined mostly by the scattering with LO phonons. Contribution of the acoustic phonon-scattering is less important for the entire temperature range for CdS. The diffusion coefficient of the electron and the hole can be calculated from the mobility using the Einstein relation employing the Maxwell distribution for the free carrier. Ambipolar diffusion coefficient D is defined as $1/D=(1/D_e+1/D_h)/2$, where D_e and D_h are the diffusion coefficients of the electron and the hole, respectively. The resultant D value is $D=13$ cm^2/s at $T_{eff}=50$ K for the neutral impurity concentration of 10^{15} cm^{-3}. The D value decreases with increasing T_{eff}, and $D=7$ cm^2/s at $T_{eff}=70$ K and $D=3$ cm^2/s at $T_{eff}=100$ K for the same impurity concentration. For larger impurity concentration the D value decreases further at low temperature, but is less affected for $T_{eff}>70$ K. The observed diffusion coefficients listed in Table I are found to be in good agreement with these calculated values. Furthermore, the observed D values at $T_{bath}=10$ K are found to be in good agreement with the ambipolar diffusion coefficient estimated from the observed Hall mobility of electrons in CdS (Refs. 11 and 17), i.e., $D\sim 9.8$ cm^2/s for $T_{eff}=40$ K.

In the above calculation, we assumed the Maxwell distribution for free carriers, which leads to the fact that the resultant D values are independent of the carrier density. This, however, is different from the experimental results where the D value becomes larger with increasing excitation density. Experimentally, the free-carrier density encountered here is too high and the temperature is too low to be expressed by the Maxwell distribution. Furthermore, the calculation was performed assuming that the free carrier is in thermal equilibrium with the lattice, i.e., $T_{eff}=T_{bath}$, which is in contradiction with the experimental results ($T_{eff}>T_{bath}$). Calculations which take these facts into consideration are required for a more detailed discussion.

The scattering matrix element between excitons and LO phonons is essentially the same as that between bare

charged particles and LO phonons, but is multiplied by factors which represent the extent of the overlap of the Wannier envelop functions involved in the scattering.[18] For the collision of a 1s exciton with the kinetic energy of $0.2\hbar\omega_{LO} \sim 2\hbar\omega_{LO}$ ($\hbar\omega_{LO} = 37.2$ meV) with an LO phonon, the scattering probability becomes about 2 orders of magnitude larger than that of free carriers with the same kinetic energy. Qualitatively speaking, the diffusion coefficient (or the mobility) is inversely proportional to the scattering probability, resulting in the fact that the diffusion coefficient of the exciton becomes about 2 orders of magnitude smaller than that of the electron or the hole. This is the reason why we ignored the exciton diffusion in calculating the diffraction intensity in Sec. II B.

V. CONCLUSION

We have demonstrated that the simultaneous detection of the decay of different diffraction orders in transient-induced grating experiments provides a detailed insight into the dynamics of excited carrier systems. With the aid of theoretical calculations we have shown the following results for CdS: Nonlinear processes such as the bimolecular recombination of electrons and holes in the degenerate plasma and the free-carrier–exciton Mott transition in the nondegenerate plasma cause the occurrence of higher-order Fourier components in the grating at low temperatures. The obtained transformation rate of $(1-1.5)\times 10^{10}$ s^{-1} is much smaller than the bimolecular recombination rate for the degenerate plasma of about 10^{11} s^{-1}.

At higher temperatures where the exciton molecule is thermally dissociated, thermal equilibrium is established between the exciton and the free carrier. The nonlinear relation between the exciton density and the free-carrier density also brings about the exciton grating with doubled period in the free-carrier grating. With further increase of the temperature, the exciton density becomes negligibly small because of thermal dissociation, and no higher-order Fourier components result.

These results demonstrate that the spatial resolution in transient-induced grating experiments can be extended to a microscopic scale by inclusion of higher diffraction orders, thus opening a new potential for the study of carrier dynamics in solids on picosecond and subpicosecond time scales.

ACKNOWLEDGMENTS

The authors thank E. O. Göbel for helpful discussions, K. Rother and H. Klann for their expert technical assistance, and S. R. Tiong for careful reading of the manuscript. H. Saito also gratefully acknowledges the financial support of the Max-Planck-Institut für Festkörperforschung, Stuttgart, Federal Republic of Germany, where the experimental work was performed.

[1]H. J. Eichler, in *Festkörperprobleme—Advances in Solid State Physics,* edited by J. Treusch (Vieweg, Braunschweig, 1978), Vol. XVIII, p. 241.

[2]A. L. Smirl, in *Semiconductors Probed by Ultrafast Laser Spectroscopy,* edited by R. R. Alfano (Academic, Orlando, Fla., 1984), Vol. 1, Sec. 7, p. 197.

[3]Y. Aoyagi, Y. Segawa, and S. Namba, in *Semiconductors Probed by Ultrafast Laser Spectroscopy,* Ref. 2, Vol. 1, Sec. 10, p. 329.

[4]H. Kalt, V. G. Lyssenko, R. Renner, and C. Klingshirn, J. Opt. Soc. Am. B **2**, 1188 (1985), and references therein.

[5]T. Takagahara, in *Semiconductors Probed by Ultrafast Laser Spectroscopy,* Ref. 2, Vol. 2, Sec. 23, p. 331.

[6]H. Saito and E. O. Göbel, Opti. Lett. **11**, 354 (1986); E. O. Göbel and H. Saito, in *Ultrafast Phenomena V,* edited by G. R. Fleming and A. E. Siegman (Springer, Berlin, 1986), p. 254.

[7]For a review on high-density phenomena in semiconductors see C. Klingshirn and H. Haug, Phys. Rep. **70**, 315 (1981); and also see Proceedings of the 3rd ICTP-IUPUP Semiconductor Symposium on High Excitation and Short Pulse Phenomena, Trieste, 1984 [J. Lumin. **30**, 1 (1985)].

[8]R. S. Knox, in *Theory of Excitons,* edited by F. Seitz and D. Turnbull, Vol. 5 of *Solid State Physics—Advances in Research and Applications* (Academic, New York, 1963), Suppl., p. 103.

[9]For material parameters in CdS see G. Beni and T. M. Rice, Phys. Rev. B **18**, 768 (1978), and references therein.

[10]W. R. Klein and B. D. Cook, IEEE Trans. Sonics Ultrason. **SU-14**, 123 (1967).

[11]H. Saito and E. O. Göbel, Phys. Rev. B **31**, 2360 (1985); H. Saito, J. Lumin. **30**, 303 (1985).

[12]H. Saito and S. Shionoya, J. Phys. Soc. Jpn. **37**, 423 (1974); A. Kuroiwa, H. Saito, and S. Shionoya, *ibid.* **45**, 1164 (1978).

[13]T. M. Rice, in *The Electron-Hole Liquid in Semiconductors: Theoretical Aspects,* edited by H. Ehrenreich, F. Seitz and D. Turnbull Vol. 32 of *Solid State Physics—Advances in Research and Applications* (Academic, New York, 1977), p. 48.

[14]Experimentally, the second-order diffraction intensity should be the sum of $I_{dif}^{(1)}(\Lambda/2)$ and $I_{dif}^{(2)}(\Lambda)$, because both diffracted beams should appear in the same diffraction direction (see Fig. 2). As already mentioned, however, the calculated value for $I_{dif}^{(2)}(\Lambda)/I_{dif}^{(1)}(\Lambda)$, which is of the order of 10^{-5}, is at least two orders of magnitude smaller than the value for $I_{dif}^{(1)}(\Lambda/2)/I_{dif}^{(1)}(\Lambda)$, which is of 10^{-3}–10^{-1} (Fig. 1). Therefore, the contribution of $I_{dif}^{(2)}(\Lambda)$ to the observed second-order diffraction intensity can be neglected.

[15]The carrier density and temperature of the plasma at the moment where its gain disappears are about 5×10^{17} cm^{-3} and 50–60 K, respectively. This density, however, is still 1 order of magnitude higher than the calculated Mott density [M. Rösler and R. Zimmermann, Phys. Status Solidi B **83**, 85 (1977)]. Then the Mott transformation may take place mainly at the low-density regions such as the wings of the grating and also inside the crystal.

[16]E. M. Conwell, in *High Field Transport in Semiconductors,* edited by F. Seitz and D. Turnbull, Vol. 9 of *Solid State Physics—Advances in Research and Applications* (Academic, New York, 1967), Suppl., p. 105.

[17]D. L. Rode, in *Semiconductors and Semimetals,* edited by R. K. Willardson and A. C. Beer (Academic, New York, 1975), Vol. 10, p. 1.

[18]Y. Toyozawa, Prog. Theor. Phys. **20**, 53 (1958).

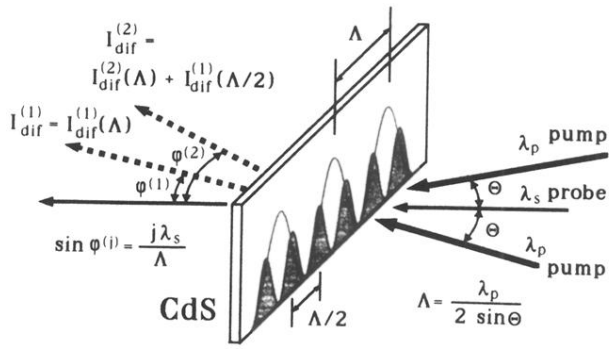

FIG. 2. Schematics of experimental technique for producing and measuring transient grating. $I^{(1)}_{dif}$ and $I^{(2)}_{dis}$ are the first- and second-order diffracted beams, respectively.